Monthly Notices of the ROYAL ASTRONOMICAL SOCIETY

MNRAS **504,** 1888–1901 (2021) doi:10.1093/mnras/stab988
Advance Access publication 2021 April 12

Interacting galaxies in the IllustrisTNG simulations – III. (The rarity of) quenching in post-merger galaxies

Salvatore Quai [1]★ Maan H. Hani [1,2]† Sara L. Ellison [1] David R. Patton [3] and Joanna Woo [4]

[1]*Department of Physics and Astronomy, University of Victoria, 3800 Finnerty Rd, Victoria, BC V8P 5C2, Canada*
[2]*Department of Physics and Astronomy, McMaster University, Hamilton, ON L8S 4M1, Canada*
[3]*Department of Physics and Astronomy, Trent University, 1600 West Bank Drive, Peterborough, ON K9L 0G2, Canada*
[4]*Department of Physics, Simon Fraser University, 8888 University Dr, Burnby, BC V5A 1S6, Canada*

Accepted 2021 April 2. Received 2021 April 1; in original form 2021 January 8

ABSTRACT

Galaxy mergers are traditionally one of the favoured mechanisms for the transformation of spiral galaxies to spheroids and for quenching star formation. To test this paradigm in the context of modern cosmological simulations, we use the IllustrisTNG simulation to investigate the impact of individual merger events on quenching star formation [i.e. star formation rate (SFR) at least 3σ below the star-forming main sequence] within 500 Myr after the coalescence phase. The rate of quenching amongst recently merged galaxies is compared with a control sample that is matched in redshift, stellar mass, SFR, black hole mass, and environment. We find quenching to be uncommon among the descendants of post-merger galaxies, with only ∼5 per cent of galaxies quenching within 500 Myr after the merger. Despite this low absolute rate, we find that quenching occurs in post-mergers at twice the rate of the control galaxies. The fraction of quenched post-merger descendants 1.5 Gyr after the merger become statistically indistinguishable from that of non-post-mergers, suggesting that mergers could speed up the quenching process in those post-mergers whose progenitors had physical conditions able to sustain effective active galactic nuclei (AGN) kinetic feedback, thus capable of removing gas from galaxies. Our results indicate that although quenching does not commonly occur promptly after coalescence, mergers none the less do promote the cessation of star formation in some post-mergers. We find that, in IllustrisTNG, it is the implementation of the AGN kinetic feedback that is responsible for quenching post-mergers, as well as non-post-merger controls. As a result of the released kinetic energy, galaxies experience gas loss and eventually they will quench. Galaxies with an initially low gas fraction show a preferable pre-disposition towards quenching. The primary distinguishing factor between quenched and star-forming galaxies is gas fraction, with a sharp boundary at $f_{\rm gas} \sim 0.1$ in TNG.

Key words: galaxies: evolution – galaxies: general – galaxies: interactions – galaxies: star formation.

1 INTRODUCTION

Galaxies show bimodal distributions in fundamental properties, such as colours and structure, both locally (e.g. Strateva et al. 2001; Blanton et al. 2003; Kauffmann et al. 2003; Baldry et al. 2004) and out to at least $z \sim 2$ (e.g. Bell et al. 2004, 2012; Willmer et al. 2006; Whitaker et al. 2011; Wuyts et al. 2011; Cheung et al. 2012; Muzzin et al. 2013). Moreover, there is strong evidence that there is continuous growth in the number density and stellar mass of the red and passively evolving early-type population from $z \sim 1$–2 to the present (e.g. Bell et al. 2004; Faber et al. 2007; Pozzetti et al. 2010; Ilbert et al. 2013). This implies that a large fraction of late-type galaxies convert into early-types due to the suppression of star formation (hereafter quenching) that accompanies their change in morphologies (e.g. Drory et al. 2004; Faber et al. 2007; Peng et al. 2010; Pozzetti et al. 2010; Tacchella et al. 2015; Woo et al. 2015). It is also thought that these transitional scenarios depend on the environment in which the galaxies are located (e.g. Goto et al. 2003; Balogh et al. 2004; Peng et al. 2010; Woo et al. 2017).

Many mechanisms have been proposed for the physical origin of star formation quenching (see e.g. the review by Somerville & Davé 2015), including (i) the heating of the inner halo gas by cosmological accretion via ram pressure drag and local shocks (i.e. gravitational quenching; Dekel & Birnboim 2008), (ii) the stability of discs against fragmentation to bound clumps (i.e. morphological quenching; Martig et al. 2009; Gensior, Kruijssen & Keller 2020; Gensior & Kruijssen 2021), (iii) the removal of the gas supply due to active galactic nuclei (AGN) activity, and/or stellar feedback (e.g. Di Matteo, Springel & Hernquist 2005; Bower et al. 2006; Sijacki et al. 2007; Cattaneo et al. 2009; Fabian 2012), (iv) the interaction between the galaxy gas with the intracluster medium in high-density environments (i.e. environmental or satellite quenching; Gunn & Gott 1972; Larson, Tinsley & Caldwell 1980; Moore, Lake & Katz 1998; Bekki 2009; Peng et al. 2010, 2012), and (v) the interaction with other galaxies (i.e. major mergers; Di Matteo et al. 2005; Springel, Di Matteo & Hernquist 2005a,c; Croton et al. 2006; Hopkins et al. 2008; Somerville et al. 2008). Quenching processes tend to be classified as internal or environmental depending on whether they

★ E-mail: squai@uvic.ca
† Herschel Fellow.

originated within a galaxy or if they are triggered by the influence of the external factors (e.g. the intracluster medium). These processes are not mutually exclusive, and they could in principle take place together on different time-scales.

AGN quenching is one of the most popularly invoked mechanisms for quenching star formation, but it remains controversial. On the one hand, several observational studies have supported the thesis that AGN feedback should be able to remove gas from the galactic reservoir, eventually leading to quenching (e.g. Kaviraj et al. 2007; Fabian 2012; Cimatti et al. 2013). The link between AGN and quenching is also supported by the theoretical results obtained combining *N*-body simulations of dark matter halo evolution (Springel et al. 2005b; Boylan-Kolchin et al. 2009) with semi-analytic models for galaxy formation (White & Frenk 1991; Springel et al. 2005b; Lu et al. 2011; Benson 2012). On the other hand, there is a growing body of literature that finds that AGN have normal gas reservoirs, both in the atomic (e.g. Ellison et al. 2019), and molecular gas phase (e.g. Shangguan, Ho & Xie 2018; Jarvis et al. 2020; Shangguan et al. 2020; Koss et al. 2021), with the possible exception of gas depletion in the dwarf regime (Bradford et al. 2018; Ellison et al. 2019). The persistence of large gas reservoirs is at odds with the scenario of AGN-driven feedback leading to quenching.

Since many models of galaxy interactions lead to AGN triggering, it has long been suggested that galaxy mergers could provide a major pathway for galaxy quenching (Di Matteo et al. 2005; Springel et al. 2005a,c; Croton et al. 2006; Hopkins et al. 2008; Somerville et al. 2008). Strong mechanical AGN feedback triggered by the inflow of gas at low angular momentum could potentially drive out the gas from the galaxy. This halts the star formation, and hampers the replenishment of the galactic gas reservoir. At the same time, theory predicts strong morphological disturbances (e.g. Di Matteo et al. 2007) that should accompany the migration from the blue cloud to the red sequence (Mihos & Hernquist 1996; Hopkins et al. 2008; Somerville et al. 2008) consistent with observations that quenched galaxies tend to have spheroidal morphologies (e.g. the review by Conselice 2014).

Given the advances in simulations over the last decade, it is worth reviewing the predicted link between mergers, AGN triggering, and quenching. Previous simulations that linked mergers to AGN activity tended to have very aggressive feedback recipes (e.g. Springel et al. 2005c; Bower et al. 2006; Hopkins et al. 2008; Khalatyan et al. 2008). However, we currently know from observations that the majority of interacting galaxies (i.e. mergers and pairs) in the local Universe show a relatively modest enhancement in both star formation and AGN luminosity (Patton et al. 2005, 2013, 2020; Ellison et al. 2008, 2013, 2019; Li et al. 2008; Jogee et al. 2009; Scudder et al. 2012; Knapen, Cisternas & Querejeta 2015; Rodighiero et al. 2015; Thorp et al. 2019). Both theoretical and observational studies agree on an increase of the major merger rate with redshift out to at least $z \sim 1.5$ (e.g. Lin et al. 2008; de Ravel et al. 2009; Lotz et al. 2011; López-Sanjuan et al. 2013; Rodriguez-Gomez et al. 2015), whilst minor mergers show little evolution with redshift (e.g. Lotz et al. 2011). However, there is no consensus on whether the contribution of galaxy mergers to star formation decreases with increasing redshift (e.g. Rodighiero et al. 2011; Wilson et al. 2019), or continue to produce enhanced star formation (e.g. Lin et al. 2007; Wong et al. 2011). Moreover, there has been no previous work to study the quenching statistics of mergers in a full cosmological setting. The work presented here investigates merger-driven quenching in an unbiased statistical galaxy sample, using a modern AGN implementation offered by the IllustrisTNG simulations (Springel et al. 2017; Marinacci et al. 2018; Naiman et al. 2018; Nelson et al. 2018, 2019; Pillepich et al. 2018b). We follow the evolution of simulated star-forming post-mergers within a realistic cosmological context. We then compare their evolution to that of non-post-merger galaxies with similar physical parameters and environment.

This paper is organized as follows. In Section 2, we introduce our methodology. In Section 3, we present the results quantifying the impact of galaxy mergers on star formation quenching. In Sections 4 and 5, we discuss the effects of our methodology on the results. Finally, we summarize our work in Section 6.

2 DATA AND METHODS

2.1 The IllustrisTNG simulation suite

The work we present here is primarily aimed at quantifying the impact of galaxy mergers on star formation quenching. We identify galaxy post-mergers in the IllustrisTNG simulation suite (Nelson et al. 2019) to study the relationship between mergers and the interruption of star formation within a cosmological framework. The IllustrisTNG project includes a suite of large-box magneto-hydrodynamical cosmological simulations in a Λ cold dark matter (ΛCDM) universe that provides an exquisite sample of galaxies spanning a variety of galaxy properties (e.g. mass, environment, star formation rate – SFR). Here we briefly summarize the main characteristics of the simulations. The simulations and physical model are introduced in detail in Marinacci et al. (2018), Naiman et al. (2018), Nelson et al. (2018), Pillepich et al. (2018b), and Springel et al. (2017). IllustrisTNG (or TNG) is the descendant of the Illustris cosmological simulation (Vogelsberger et al. 2013, 2014) with an improved physical models and numerical scheme. Moreover, TNG introduces a number of additional features to obtain a better agreement with observational results. In this paper, we focus on TNG300-1, the highest resolution run for the largest publicly released volume of 302^3 cMpc^3. TNG300-1 offers the largest statistics, whilst still guaranteeing adequate numerical resolution. TNG300-1 has 2500^3 initial resolution elements, with dark matter and stellar mass resolutions of 5.9×10^7 and 1.1×10^7 $M_\odot$, respectively. The simulation runs from redshift 127 to the present day using the AREPO moving-mesh code (Springel 2010; Pakmor et al. 2016). The cosmological parameters used in IllustrisTNG are in accordance with Planck Collaboration XIII (2016) that is given by a matter density $\Omega_{M,0} = 0.3089$, baryon density $\Omega_{b,0} = 0.0486$, dark energy density $\Omega_{\Lambda,0} = 0.6911$, and a Hubble parameter $h = 0.6774$. For our purposes, it is relevant to introduce some features of the IllustrisTNG physical model.

(i) *Star formation*. Star formation occurs in a pressurized, multi-phase interstellar medium (ISM) following the Springel & Hernquist (2003) formalism. Gas particles whose density exceeds a threshold of $\sim$0.1 cm^{-3} are 'star forming' and their gas is converted to stars stochastically following the Schmidt–Kennicutt law (Kennicutt 1998) assuming a Chabrier (2003) initial mass function (see Nelson et al. 2015; Pillepich et al. 2018a, for further details).

(ii) *Black holes and AGN feedback*. Black holes are seeded with an initial mass of 1.18×10^6 $M_\odot$ at the centres of the potential wells of haloes exceeding a threshold mass of 7.38×10^{10} $M_\odot$. Black holes can grow their mass either through (1) accretion following the modify Bondi–Hoyle scheme, or (2) mergers with other black holes. AGN feedback is directly related to the accretion rate on to the central black holes ($\dot{E} \propto \dot{M}_{\rm BH}\, c^2$). At high accretion rates (i.e. quasar mode feedback), thermal energy is returned to the black hole's environment, whereas at low accretion rates (i.e. radio mode

feedback, or kinetic feedback), energy accumulates until it reaches an energy threshold, then mechanical energy is instantaneously released along a random direction into the gas around the black hole (see Weinberger et al. 2017, for further details).

In the work presented here, each galaxy is parametrized by the following.

(i) *Galactic radius* ($R_{\rm gal}$). We define a galaxy's radius to be twice the stellar half-mass radius.
(ii) *Stellar mass* (M_*). The sum of the masses of all stellar particles contained within $R_{\rm gal}$ from a galaxy's centre (which is defined as the position at the minimum of the gravitational potential).
(iii) *Gas mass* ($M_{\rm gas}$). The gas mass is measured by summing the mass of all gas particles within $R_{\rm gal}$ from the galaxy's centre.
(iv) *Black hole mass* ($M_{\rm BH}$). The mass of the supermassive black hole at the minimum of a galaxy's potential well.
(v) *SFR*. This is the instantaneous star formation rate (SFR) within $R_{\rm gal}$. We use a metric based on the SFR to select and analyse the TNG post-merger galaxies. Specifically, we fit a redshift-dependent star-forming main sequence (SFMS) to the TNG sample, and define quenched galaxies as those lying at least below -3σ from the SFMS.
(vi) *Cumulative kinetic feedback* ($\int \dot{E}_{\rm kinetic}\,{\rm d}t$). In our analysis we use the total amount of kinetic AGN feedback energy injected into the gas surrounding the central black hole in the low accretion rate mode, accumulated over the entire lifetime of the black hole in the centre of the galaxy. During black hole mergers the cumulative kinetic energy is summed for the two merging components.
(vii) *Potential* ($V(r_{\rm gas})$). The gravitational potential energy experienced at the position of a gas cell ($r_{\rm gas}$), representing the energy required to unbind the gas. $V(r_{\rm gas})$ is used to calculate the total gravitational binding energy of the gas particles as in Terrazas et al. (2020):

$$E_{\rm binding}(\leq R_{\rm gal}) = \frac{1}{2}\sum_{\leq R_{\rm gal}} m_{\rm gas}\,V(r_{\rm gas}), \tag{1}$$

where the sum is extended to all the gas particles ($m_{\rm gas}$) within $R_{\rm gal}$. The total binding energy defines the amount of energy that is needed to void a galaxy of the gas within $R_{\rm gal}$.

2.2 Star-forming post-mergers

We use the post-merger galaxy sample identified in Hani et al. (2020), wherein galaxy mergers are defined as nodes in the SUBLINK merger trees (Rodriguez-Gomez et al. 2015). Namely, we define a post-merger (or PM) in the snapshot immediately after the coalescence phase as the remnant of two interacting galaxies. Given the time resolution of the TNG snapshots, this approach identifies mergers within ∼160 Myr after coalescence (i.e. the average time between successive snapshots at $z < 1$). Following Hani et al. (2020), our post-merger sample is restricted to those satisfying the following criteria.

(i) $z \leq 1$. We only follow the redshift evolution of post-mergers in the last ∼8 Gyr.
(ii) $M_* \geq 10^{10}$ M$_\odot$. In IllustrisTNG, galaxies are well resolved above $M_* > 10^9$ M$_\odot$ (i.e. ≥90 stellar particles per galaxy at the resolution of TNG 300-1). Therefore, our criterion ensures a complete sample of post-mergers with mass ratio (secondary/primary) larger than 1:10.
(iii) The mass ratio (secondary/primary, μ) in the range $0.1 \leq \mu \leq 1$.

We prevent numerical stripping issues by adopting the maximum stellar mass over the past 0.5 Gyr for all mass ratio calculations following Patton et al. (2020).
(iv) The relative separation from the nearest neighbour $r_{\rm sep} \geq 2$. The parameter $r_{\rm sep}$ is defined by Patton et al. (2020) as

$$r_{\rm sep} = \frac{r}{R_{1/2}^{\rm host} + R_{1/2}^{\rm comp}}, \tag{2}$$

where r is the 3D separation between the centres of the host (i.e. post-merger in our case) and its closest neighbour, and $R_{1/2}^{\rm host}$ and $R_{1/2}^{\rm comp}$ are the stellar half-mass radii of the post-merger and the closest neighbour, respectively. The criterion $r_{\rm sep} \geq 2$ avoids post-mergers that are undergoing further close interactions that could interfere with the descendant's evolution.
(v) The time elapsed since the previous merger must be larger than 2 Gyr, i.e. we exclude post-mergers that have experienced another merger within the last 2 Gyr. This criterion reinforces our purpose of isolating the effect of a single merger on galaxy evolution.
(vi) Galaxies must be star forming when first selected (in order that we can later observe them quenching). In practice this is implemented by requiring SFRs higher than -1σ from the star-forming main-sequence best fit. Unlike the original sample by Hani et al. (2020) who include passive post-mergers, in the work presented here, we are interested in star-forming post-mergers in order that we may track whether the merger causes them to quench. Given the arbitrary choice of our SFR threshold value, we investigate the impact of imposing different limits to separate quenched and star-forming galaxies in Section 3.

Our selection criteria yield a sample of 3472 star-forming post-mergers with stellar masses $10^{10} \leq M_*/{\rm M}_\odot \leq 10^{10.8}$, at redshift $z \leq 1$. We note that $\lesssim$10 per cent of post-mergers in our sample have a mass ratio $\mu > 0.5$, therefore the results we present in this paper are statistically dominated by minor mergers ($\mu < 0.3$).

2.3 Statistical control sample

We are interested in investigating the link between galaxy mergers and the quenching of star formation. We quantify the impact of galaxy mergers on the quenching of star formation using an observational approach that consists of identifying control galaxies that are matched to each post-merger galaxy in redshift, stellar mass, local density, and isolation (e.g. Ellison et al. 2013; Patton et al. 2013). In this section, we describe the steps of creating the control sample.

We implement an adaptation of the matching procedure used in Patton et al. (2016, 2020) to select statistical controls (CTRL) for galaxies in our sample (see also Hani et al. 2020). For each star-forming post-merger, we first define a star-forming control pool (i.e. non-post-merger galaxies with SFR higher than -1σ from the SFMS), in the same snapshot (i.e. same redshift), with $M_* \geq 10^{10}$ M$_\odot$, and a relative separation from the nearest neighbour $r_{\rm sep} \geq 2$. We then reject galaxies that have experienced a merger ($\mu \geq 0.1$) within 2 Gyr (i.e. $t_{\rm PM} \geq 2$ Gyr). Then, for each post-merger in our sample, we identify the control galaxies that match the post-merger properties as follows.

(i) $\log(M_*)$ within a tolerance of 0.05 dex.
(ii) The environmental parameters N_2 and r_1, defined by Patton et al. (2016) as the number of neighbours within a radius of 2 Mpc (i.e. local density), and the distance to the nearest neighbour with $M_* \geq 0.1 \times M_{*,\,\rm host}$ (i.e. isolation), respectively, within a tolerance of 10 per cent.

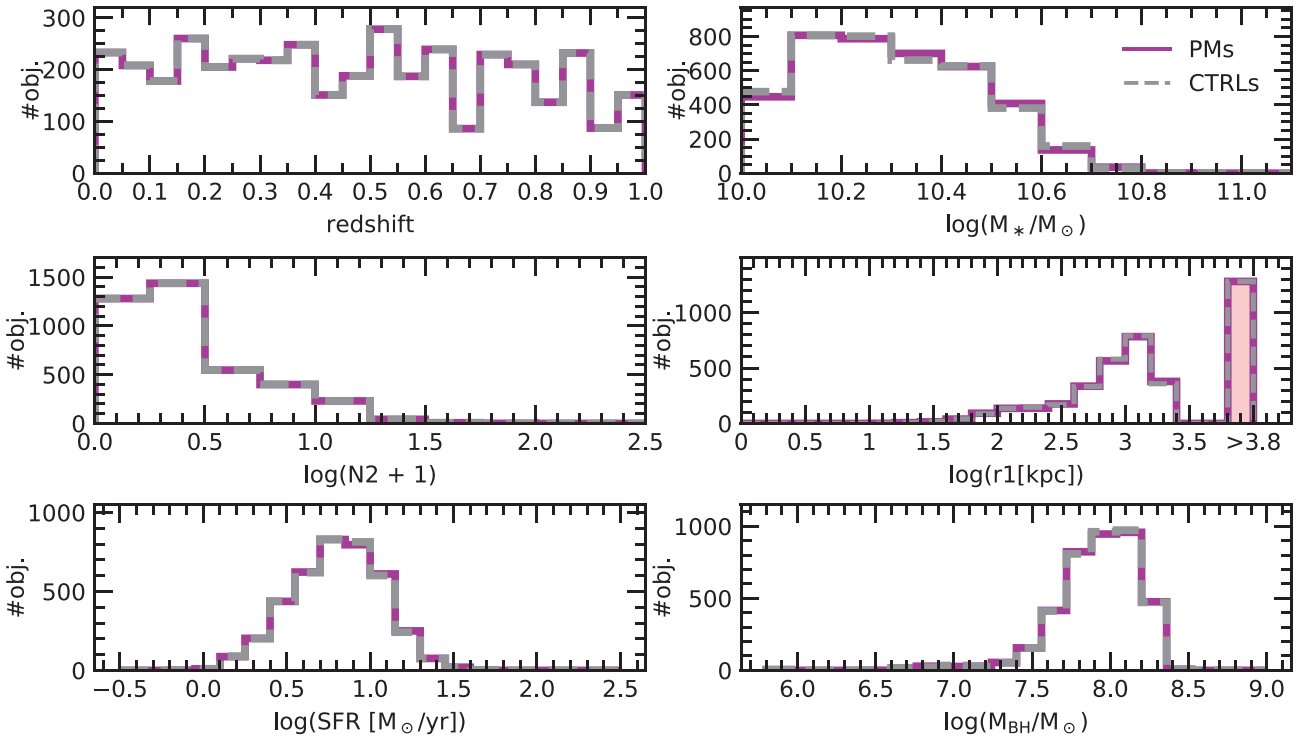

Figure 1. A comparison between the distributions of redshift, M_*, N_2, r_1, SFR, and M_{BH} of post-mergers (magenta) and their control galaxies (grey). The pink shaded bin in the $r1$ distribution includes all galaxies with $r_1 > 2$ Mpc. The control sample is very well matched to the post-merger one in all the six parameters.

(iii) log(SFR) within a tolerance of 0.01 dex.

(iv) log(M_{BH}) within a tolerance of 0.05 dex. By matching in black hole mass we prevent possible bias related to the AGN feedback model (see Section 3.3). In Section 4, we discuss how this requirement affects our results.

If more than one control is found for a given post-merger, we follow the weighting scheme of Patton et al. (2016) to select up to five control galaxies. We then define the post-merger's *control galaxy* as the single best control galaxy that shares the most number of subsequent snapshots with the post-merger's descendants whilst maintaining environmental parameters within 40 per cent of the descendants'. Fig. 1 shows the distributions of redshift, M_*, N_2, r_1, SFR, and M_{BH} for the star-forming post-mergers and their control galaxies. The matching process offers a control population that well matches our post-merger sample in all the aforementioned parameters.

Once the control galaxy sample has been identified, we follow the evolution of the SFR in descendants of post-mergers and controls forward in time through the simulation. For each galaxy, we evaluate the relative relevance of star formation by calculating, on a logarithmic scale in the SFR–M_* plane, the vertical offset between its SFR and the SFMS (hereafter ΔSFR). Then, we define galaxies to be quenched when their ΔSFR drops below -0.9 dex (i.e. a deviation of $<-3\sigma$ from the SFMS). Fig. 2 shows the evolution of ΔSFR as a function of time since merger (t_{PM}) for three example post-mergers and their controls.[1] The top panel shows a post-merger that remains star forming after coalescence, while its matched control galaxy quenches around 2.4 Gyr after $t_{PM} = 0$. The central panel shows a post-merger that quenches within 500 Myr after the merger. Finally, the bottom panel depicts a post-merger that remains star forming up to 1 Gyr after the merger, then quenches, though not permanently (i.e. it experience some episodes of low SFR). The control galaxy, instead, keeps forming stars for the entire period over which we follow its evolution (i.e. at $z = 0$).

We quantify the effects of mergers on star formation quenching using two metrics: (i) the fraction of post-merger descendants with quenched star formation; and (ii) the number of quenched post-mergers (#Q_{PM}) normalized by the number of quenched controls (#Q_{CTRL}) in 160 Myr intervals (Q_{excess}):

$$Q_{excess} = \frac{\#Q_{PM}}{\#Q_{CTRL}}. \quad (3)$$

Q_{excess} measures the relative tendency of mergers to experience quenching compared to other evolutionary processes that are accounted for in the controls. Taken together, these two metrics allow us to quantify both the absolute rate of quenching in post-mergers and assessing whether quenching happens more frequently in post-mergers that in controls.

3 RESULTS AND DISCUSSION

3.1 Quenching in descendants of star-forming post-mergers

In this section, we analyse the impact of mergers on the interruption of star formation during the early stages after the coalescence phase. We apply the methods defined in Section 2.3 to quantify differences between the evolution of star-forming post-mergers and matched control galaxies that have not experienced any merger in the past 2 Gyr. The top panel in Fig. 3 shows the evolution of the total number of post-mergers and their associated controls as a function of time elapsed since coalescence (t_{PM}), in bins of 160 Myr. The

[1] When we express the time evolution of control galaxies in terms of t_{PM}, we measure the time relative to their matched post-mergers.

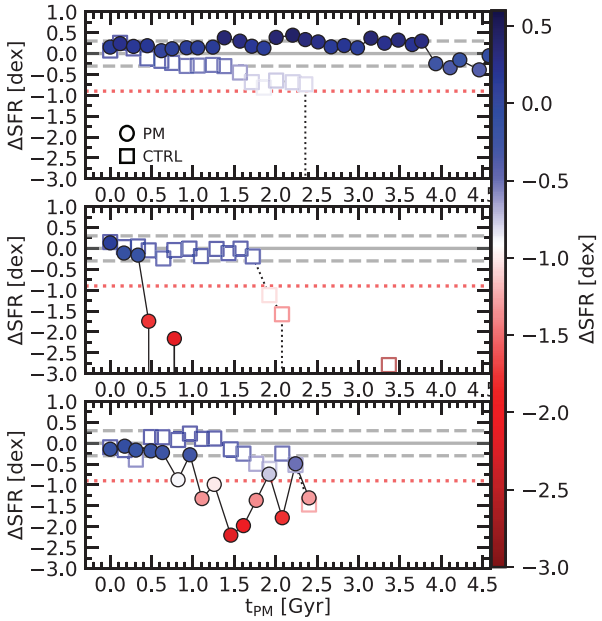

Figure 2. Examples of the evolution of ΔSFR after the merger for three example star-forming post-mergers (filled symbols) and their controls (open symbols). The colour shading represents the ΔSFR: shades of blue for ΔSFR ≥ -0.9, and reds for quenched descendants with ΔSFR < -0.9. The two dashed grey lines represent the scatter (ΔSFR ± 0.3 dex, i.e. $\pm 1\sigma$) around the SFMS (solid grey line). The red line (ΔSFR $= -0.9$ dex, i.e. -3σ below the SFMS) represents the threshold that separates star-forming (above the line) and quenched (below the line) galaxies. The top panel shows a post-merger that remains star forming after coalescence, while its matched control galaxy permanently quenches around 2.4 Gyr after $t_{PM} = 0$, as its ΔSFR stays steadily below -3 dex until redshift z =0. The central panel shows a post-merger that quenches within 500 Myr after the merger, while its matched control galaxy quenches around 2 Gyr after $t_{PM} = 0$. Finally, the bottom panel depicts a post-merger that remains star forming up to 1 Gyr after the merger, then quenches, though not permanently (i.e. it experience some episodes of low SFR). The control galaxy, instead, keeps forming stars for the entire period over which we follow its evolution (i.e. at $z = 0$). The post-merger and control galaxy evolution depicted in the bottom panel end at ∼2.5 Gyr after $t_{PM} = 0$, when the simulation reaches redshift $z = 0$.

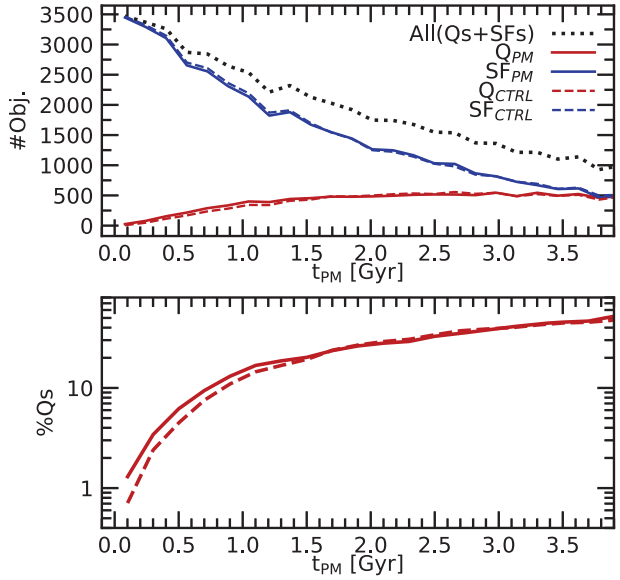

Figure 3. Top: the black dotted curve represents the total number of post-mergers (and an equal number of control galaxies) as a function of time elapsed since coalescence (t_{PM}); the solid curves represent the evolution of the number of post-mergers that are still star forming (SF_{PM}, solid blue) or quenched (Q_{PM}, solid red), respectively. The dashed curves represent the evolution of the number of still star-forming control galaxies (SF_{CTRL}, dashed blue) and quenched controls (Q_{CTRL}, dashed red), respectively. Bottom: the percentage of Q_{PM} galaxies (solid red curve) and of Q_{CTRL} galaxies (dashed red curve) as a function of t_{PM}. The figure demonstrates that the absolute fraction of quenched post-mergers are small shortly after coalescence, indicating that the merger does not promptly truncate star formation.

black dotted curve represents the total number of post-mergers (and, by definition, an equal number of control galaxies) in each bin. The total number of galaxies decreases with time for three reasons: (1) the merger rate increases with increasing redshift (e.g. Lin et al. 2008; Lotz et al. 2011); (2) we analyse the post-mergers in the range $0 \leq z \leq 1$, therefore the maximum time after the merger that we can analyse decreases as the snapshots approach $z = 0$; and (3) we only follow the evolution of a given post-merger up to the moment when its descendant, or the descendant of its control galaxy, experiences a new close encounter or a merger. We also interrupt tracing the evolution when the match between the environmental parameters (i.e. $N2$ and $r1$) exceeds a tolerance of 40 per cent. We divide the post-merger population, at any given time, into those that are star forming and those that are quenched (recalling that we require the post-mergers to be star forming at $t_{PM} = 0$). Fig. 3 shows that, in the early phase after the merger, the vast majority of post-mergers remain star forming, with only a small fraction of them becoming quenched (e.g. ∼50/3500 at t_{PM} =125 Myr). The control sample shows a qualitatively similar behaviour but with an even smaller number of quenched systems at $t_{PM} < 1$ Gyr. The bottom panel of Fig. 3 provides a complementary perspective by showing these results as percentages of each population. We find that only 1.4 per cent of the star-forming post-mergers quench their star formation within 125 Myr following coalescence, compared to 0.7 per cent for the controls. The fraction of quenched post-mergers rise to ∼5 per cent at $t_{PM} = 500$ Myr (3.5 per cent for the controls) and 16 per cent within 1 Gyr from the merger (12.5 per cent for the controls). After 1.5 Gyr the fraction of quenched post-mergers and control galaxies grow together with no appreciable distinction. We conclude from Fig. 3 that the process of coalescence does not result in widespread quenching of the post-merger population. None the less, the quenched fraction is slightly larger (an effect we quantify shortly) in the post-merger sample compared to the controls at $t_{PM} \leq 1.5$ Gyr, which may be indicative of the *subtle* effects of galaxy mergers on the quenching of merger descendants, which provide a low level facilitation of the quenching process.

In Fig. 4, we quantify the enhancement in quenched post-mergers relative to their controls as the ratio of quenched post-mergers to quenched control galaxies. It is important to stress that $t_{PM} = 0$ is not displayed in Fig. 4. By construction, we selected star-forming post-mergers and star-forming control galaxies, therefore there are 0 quenched post-mergers and control galaxies at $t_{PM} = 0$. Around 150 Myr after coalescence, we find that post-mergers are quenched with an excess of 1.83 ± 0.47 compared to their controls that have not experienced a recent merger (within the past 2 Gyr). The error is quantified as the propagation of the Poissonian 1σ error of the ratio in equation (3). The excess is confirmed at a significance level of 1.8σ, with respect to $\#Q_{PM}/\#Q_{CTRL} = 1$. We find that the excess is larger in the early post-merger phase when the mergers' effects are stronger (e.g. Hani et al. 2020), and then it decreases steadily towards $\#Q_{PM}/\#Q_{CTRL} = 1$. Beyond 1.5 Gyr after the merger, the number

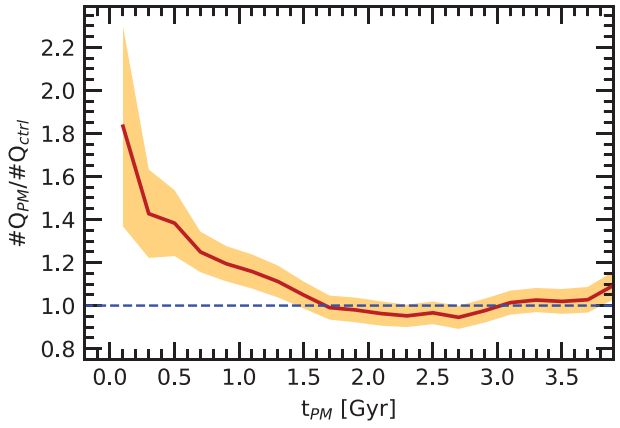

Figure 4. The ratio between the number of quenched post-mergers and quenched control galaxies as a function of the time elapsed since coalescence $t_{\rm PM}$. The shaded contours represent the error, that is quantified as the propagation of the Poissonian 1σ error of the ratio. The figure demonstrates that post-mergers show an excess of quenched galaxies, relative to expectations from the control of up to a factor of $\sim$2. The excess of quenched galaxies persists for approximately 1.5 Gyr after the merger.

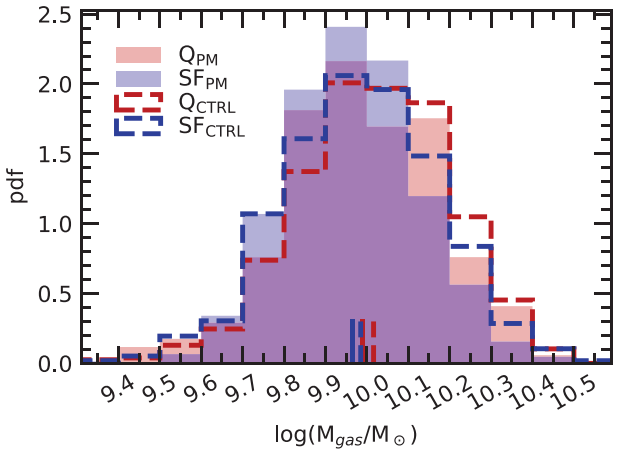

Figure 5. Distributions of the gas mass at $t_{\rm PM} = 0$. The post-mergers are represented by filled histograms: red for post-mergers that will quench within 500 Myr after coalescence ($Q_{\rm PM}$ galaxies), and blue for post-mergers that keep forming stars at least 500 Myr after coalescence ($\rm SF_{PM}$ galaxies). Control galaxies are represented by the dashed open histograms: red for control galaxies that will quench ($Q_{\rm CTRL}$ galaxies), and blue for control galaxies that keep forming stars ($\rm SF_{CTRL}$). The vertical coloured ticks around the bottom/centre of the distributions indicate the median of the respective distributions. The figure shows that, at $t_{\rm PM} = 0$, our four populations ($Q_{\rm PM}$, $\rm SF_{PM}$, $Q_{\rm CTRL}$, and $\rm SF_{CTRL}$) have very similar distributions of gas.

of quenched post-mergers becomes statistically indistinguishable from that of the control sample. We speculate that this short-term enhancement of quenched post-mergers is the result of the merger expediting quenching in a system that was already close to achieving the conditions necessary for halting star formation (i.e. a critical AGN feedback). We return to this in Section 3.3.

In order to test whether our results presented in Figs 3 and 4 depend on our definition of quenched and star-forming galaxies, we investigate the impact of different ΔSFR thresholds. Recall that since we find that the scatter around the SFMS is of $\sim$0.3 dex at any given snapshot (in accordance with observational results), our fiducial threshold for labelling a galaxy as quenched is $\Delta\rm SFR < -0.9$ to be quenched (i.e. below -3σ from the SFMS). In TNG this threshold corresponds to a specific SFR (i.e. $\log_{10}\rm SFR/M_*$) of about -11 yr^{-1}, a limit often used in observational studies to separate passive galaxies from star-forming ones (e.g. Ilbert et al. 2010, 2013; Pozzetti et al. 2010). We rerun our analysis by applying both less conservative thresholds (-2σ from the SFMS) and more conservative ones (-4σ and -5σ from the SFMS), and we do not find a significant difference in the main result presented in this section.

In the next two subsections, we will explore the properties of the post-mergers that do/do not quench. In order to distinguish a quenching event that can plausibly be linked directly to the merger, we redefine the quenched post-merger sample as those galaxies that quench within 0.5 Gyr after coalescence (171 galaxies), i.e. we remove from the $Q_{\rm PM}$ sample the 589 post-mergers that quench on time-scales longer than 0.5 Gyr. Since none of the control galaxies have experienced a significant merger within at least 2 Gyr (by definition), all of the quenched controls are retained in the $Q_{\rm CTRL}$ sample (772 galaxies). Thus, the $Q_{\rm PM}$ and $Q_{\rm CTRL}$ samples represent galaxies that have/have not quenched as the result of a recent merger. The star-forming samples ($\rm SF_{PM}$ and $\rm SF_{CTRL}$) also remain unchanged and contain 2114 and 2102 galaxies, respectively. These are the samples used in the following subsections.

3.2 Gas evolution in TNG post-mergers and control galaxies

Altering the absolute gas content, or its spatial distribution, is a possible mechanism for driving quenching. In the literature, processes that remove gas from the reservoir of star-forming galaxies are described as *ejective* feedback, while those that slow down the cooling of gas or halt gas inflow from the haloes surrounding galaxies are described as a *preventive* feedback (e.g. Somerville & Davé 2015). In practice, quenching could result from both types of feedback. In this section, we explore the evolution of the amount of gas in the reservoir of TNG post-mergers, to understand what kind of feedback leads to the quenching of star formation. Moreover, we explore whether the process(es) that drive quenching are the same in the quenched post-mergers (i.e. $Q_{\rm PM}$) and quenched control galaxies (i.e. $Q_{\rm CTRL}$).

To analyse the nature of the feedback responsible for quenching in post-merger galaxies, we start by studying the evolution of gas in quenched post-merger galaxies and in the other three samples. In Fig. 5, we show the distribution of the amount of gas at $t_{\rm PM} = 0$ in quenched post-mergers ($Q_{\rm PM}$), quenched control galaxies ($Q_{\rm CTRL}$), star-forming post-mergers ($\rm SF_{PM}$), and star-forming control galaxies ($\rm SF_{CTRL}$). At $t_{\rm PM} = 0$, the four subsamples have similar gas masses between $10^{9.4}$ and $10^{10.55}$ $\rm M_\odot$, with over 50 per cent of galaxies possessing a gas mass larger than $10^{9.95}$ $\rm M_\odot$.

We quantify the fractional change in gas mass between $t_{\rm PM} = 0$ (or t_0) and the time at which a galaxy quenches ($t_{\rm Q}$) as follows:

$$\Delta \text{ per cent}\,[M_{\rm gas}] = \frac{M_{\rm gas}(t_{\rm Q}) - M_{\rm gas}(t_0)}{|M_{\rm gas}(t_0)|} \times 100. \quad (4)$$

Since we select the $\rm Q_{CTRL}$ subsample without any constraints on the time of the quenching (see Section 3.1), several $\rm Q_{CTRL}$ galaxies quench on very long ($\gtrsim$Gyr) time-scales. Therefore, we calculate Δ per cent $[M_{\rm gas}]$ for the $\rm Q_{CTRL}$ sample relative to their gas mass $\sim$500 Myr before they quench that is consistent with the time-scale used for comparison for the post-merger sample. For the $\rm SF_{PM}$ (and $\rm SF_{CTRL}$), we instead evaluate Δ per cent $[M_{\rm gas}]$ at the third snapshot after coalescence (i.e. $\sim$500 Myr). The red coloured histogram in Fig. 6 shows the Δ per cent $[M_{\rm gas}]$ distributions for the quenched post-merger galaxies ($Q_{\rm PM}$). We find that all $Q_{\rm PM}$ galaxies have at least 25 per cent less gas than their

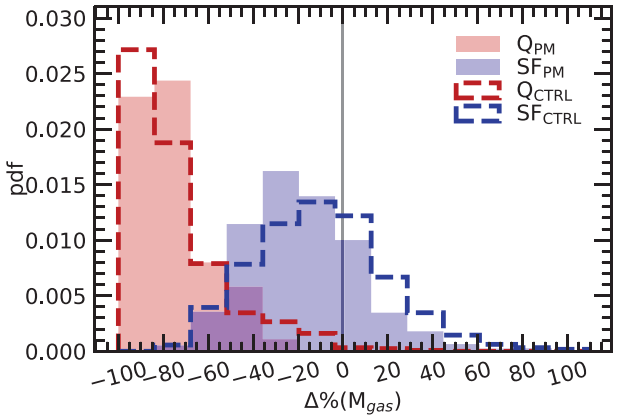

Figure 6. Distributions of the gas percentage change in galaxies (Δ per cent $[M_{\rm gas}]$). Δ per cent $[M_{\rm gas}]$ represents the percentage of gas lost with respect to the gas distribution shown in Fig. 5. The post-mergers are represented by filled histograms: red for quenched post-mergers ($Q_{\rm PM}$ galaxies), and blue for star-forming post-mergers ($\rm SF_{PM}$ galaxies). Control galaxies are represented by the dashed open histograms: red for quenched control galaxies ($Q_{\rm CTRL}$ galaxies), and blue for star-forming control galaxies ($\rm SF_{CTRL}$). The vertical grey line separates galaxies with a net gas loss (left) from those with a net gas gain (right). The figure demonstrates that quenching in post-mergers is characterized by a large fractional gas loss, and that there is neither a substantial difference between gas loss in $Q_{\rm PM}$ and $Q_{\rm CTRL}$ galaxies nor between $\rm SF_{PM}$ and $\rm SF_{CTRL}$ galaxies.

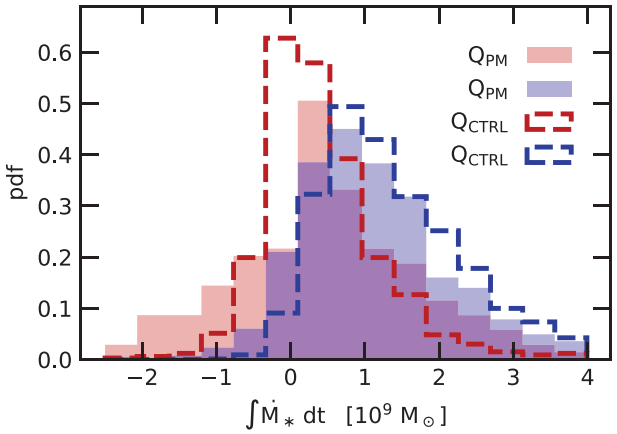

Figure 7. Distributions of stellar mass growth measured in the same interval of time as for Fig. 6. The post-mergers are represented by filled histograms: red for quenched post-mergers ($Q_{\rm PM}$ galaxies), and blue for star-forming post-mergers ($\rm SF_{PM}$ galaxies). Control galaxies are represented by the dashed open histograms: red for quenched control galaxies ($Q_{\rm CTRL}$ galaxies), and blue for star-forming control galaxies ($\rm SF_{CTRL}$).

initial amount. However, 68 per cent of them (between 16th and 84th percentile) experienced a much larger gas removal in the range between 60 per cent and 92 per cent and a median loss of 82 per cent of the initial gas mass. The distribution of quenched post-merger galaxies shows remarkable similarity with that of the quenched control galaxies sample (red dashed histogram), thus suggesting that quenching is not special in post-mergers, and that it is characterized by gas loss in both post-mergers and controls. Fig. 6 also shows the gas percentage change of the star-forming post-merger population ($\rm SF_{PM}$, blue coloured histogram) and star-forming control population ($\rm SF_{CTRL}$, blue dashed histogram). These two star-forming subsamples show distributions of Δ per cent $[M_{\rm gas}]$ different from those of the quenched galaxies: the median values for $\rm SF_{PM}$ and $\rm SF_{CTRL}$ galaxies are Δ per cent $[M_{\rm gas}] = -25$ per cent and -10 per cent, respectively, and almost 25 per cent of $\rm SF_{PM}$ and 35 per cent of $\rm SF_{CTRL}$ galaxies have even accreted gas mass (Δ per cent $[M_{\rm gas}] > 0$) with respect to the initial amounts.

Possible reasons for the decline in the measured gas mass in galaxies include (1) conversion of gas into stars, and (2) the gas has been moved beyond $R_{\rm gal}$. Considering the case of gas conversion into stars, this would require converting $\sim 8 \times 10^9$ $\rm M_\odot$ of gas into stars in about 500 Myr, equivalent to a steady SFR ≥ 15 $\rm M_\odot$ $\rm yr^{-1}$. Although post-merger galaxies show particularly enhanced star formation activity, their starburst phase lasts for only some tens Myr after coalescence and then their SFR drops exponentially to a more typical star-forming level (e.g. Hani et al. 2020). Fig. 7 shows the stellar mass growth distributions in our four subsamples, measured in the same interval of time as for Fig. 6. In the interval of time between the merger and quenching, the stellar mass in quenched post-merger galaxies increases, on average, by $\sim 10^{8.7}$ $\rm M_\odot$, with a maximum of $\sim 10^{9.3}$ $\rm M_\odot$. This amount of new stellar mass is far lower the measured loss in gas mass. For example, we find that quenched post-mergers that show an increment in stellar mass of $\sim 10^{8.7}$ $\rm M_\odot$ have experienced a gas loss in the range $10^{9.5}$–$10^{10.1}$ $\rm M_\odot$ (i.e. 16th–84th percentiles), with a median gas loss of $10^{9.8}$ $\rm M_\odot$.

We do not find a significant difference between quenched post-mergers and quenched control galaxies. Thus, we can rule out the conversion into stars as a cause of the observed reduction of gas in quenched galaxies, which instead can be only explained by gas ejected from the galaxy beyond $R_{\rm gal}$. We also find that 70.8 ± 8.4 per cent of quenched post-merger galaxies remain quenched for the rest of the simulation (i.e. up to $z = 0$), 22.8 ± 4 per cent of them exhibit only sporadic episodes of low SFRs and only around 6.4 ± 2 per cent of the quenched post-merger galaxies rejuvenate. These numbers are in accordance with the evolution of the quenched control population, with 72.4 ± 4 per cent permanently quenched, 15.8 ± 1.5 per cent that show some episodes of low star formation, and 11.8 ± 1.3 per cent that return to the star-forming main sequence. The aforementioned results suggest that the mechanism responsible for the gas removal must also be responsible for preventive feedback, which would explain the lack of rejuvenation.

We showed earlier in this section that the star-forming post-merger and control populations experience less gas mass loss than quenched post-merger and control galaxies (see Fig. 6), therefore, this would require converting ~ 1–2×10^9 $\rm M_\odot$ of gas into stars in about 500 Myr. Fig. 7 reveals that ~ 49.5 per cent of star-forming post-mergers and ~ 60 per cent of star-forming control galaxies have increased their stellar mass of at least 1×10^9 $\rm M_\odot$ over 500 Myr, an amount consistent with the measured gas loss.

In this section, we showed that both quenched post-merger and control galaxies show high rates of gas loss and a high fraction of permanent quenching. This common behaviour supports a scenario where the vast majority of both quenched post-mergers and quenched control galaxies are quenched because of a common feedback process that ejects the gas out of galaxies and prevents its further accretion by either supplying kinetic energy to the remaining medium or by increasing the entropy of the ejected gas and prolonging its cooling time (see Zinger et al. 2020). In the next section, we focus on the quenching mechanism in the quenched post-merger population and we compare the outcome with that of the quenched control galaxies, in order to understand the origin of the excess of quenched post-mergers in the early times after the coalescence phase.

3.3 The impact of AGN feedback

In the previous section, we showed that gas loss is the cause of quenching in post-merger galaxies, as well as controls, which suggests that ejective quenching mechanisms are responsible for the gas loss in both samples. In this section, we explore the possibility that different mechanisms are responsible for the quenching in the post-mergers and control quenched galaxies. In Section 2.1, we briefly described the AGN feedback implemented in TNG model. To recap, the TNG AGN model feedback employs either pure kinetic feedback at low accretion rates, or thermal feedback at high accretion rates. This scheme is in accordance with the two modes of activity in observed AGN (e.g. Crenshaw et al. 2010; Villar-Martín et al. 2011; Woo et al. 2016, for the high accretion mode, and McNamara & Nulsen 2007; Fabian 2012, for the low accretion mode), with improved agreement with the observational results regarding coevolution of galaxies and black holes (Weinberger et al. 2017, 2018). At high accretion rates, the TNG model injects pure thermal energy into the gas surrounding the black hole. However, Weinberger et al. (2017) show that such energy does not efficiently couple with the gas, resulting in almost unaltered thermodynamics of the TNG gas cells, with no or insufficient impact on the cooling/heating functions and, therefore, on the star formation in TNG galaxies (Weinberger et al. 2017; Terrazas et al. 2020). To simulate the feedback at low accretion rates, instead, TNG uses a kinetic wind model. The energy accumulates proportionally to the accretion rate until a threshold amount is reached. Then, the kinetic energy is released impulsively into the gas surrounding the black hole in a random direction (Weinberger et al. 2017).

Studies of quenching in IllustrisTNG (Weinberger et al. 2017; Nelson et al. 2018; Terrazas et al. 2020) reveal that only the kinetic mode of AGN feedback offers the necessary conditions to suppress the star formation in TNG galaxies with $M_* \geq 10^{10}$ M$_\odot$, by pushing gas away from the galaxy. Moreover, Terrazas et al. (2020) demonstrate that the ejective feedback in TNG becomes effective at quenching star formation once the cumulative kinetic energy overcomes the total gravitational binding energy of the gas in a galaxy. They also show that the kinetic feedback process dominates in galaxies whose $M_{\rm BH}$ exceeds $10^{8.2}$ M$_\odot$, the black hole mass threshold above which more than 90 per cent of the TNG galaxies are quenched (see also Zinger et al. 2020). This $M_{\rm BH}$ threshold for quiescence arises from the TNG model parameters chosen to reproduce observational properties of the galaxy population at the present time (Pillepich et al. 2018a).

In the top panel of Fig. 8, we investigate the role of the AGN on quenching in our post-merger sample by showing the correlation between the cumulative kinetic energy released into the gas and the central black hole mass. Most of the quenched post-mergers sample galaxies occupy the high $M_{\rm BH}$ regime $M_{\rm BH} \geq 10^{8.2}$ M$_\odot$ and also have the largest cumulative kinetic energies. The star-forming post-merger galaxies instead preferentially have $M_{\rm BH} < 10^{8.2}$ M$_\odot$ and exhibit a wide range of cumulative kinetic energies. The behaviour of the TNG controls is broadly consistent with that of the quenched and star-forming post-merger populations, although quenched post-merger galaxies have slightly larger $M_{\rm BH}$ than quenched control galaxies, with ∼80 per cent of quenched post-mergers exceeding the threshold of $M_{\rm BH} = 10^{8.2}$ M$_\odot$, whereas only ∼60 per cent of the quenched control galaxies have larger $M_{\rm BH}$ than the threshold value. Therefore neither the black hole mass threshold nor a large amount of cumulative kinetic feedback is sufficient conditions for quenching TNG galaxies.

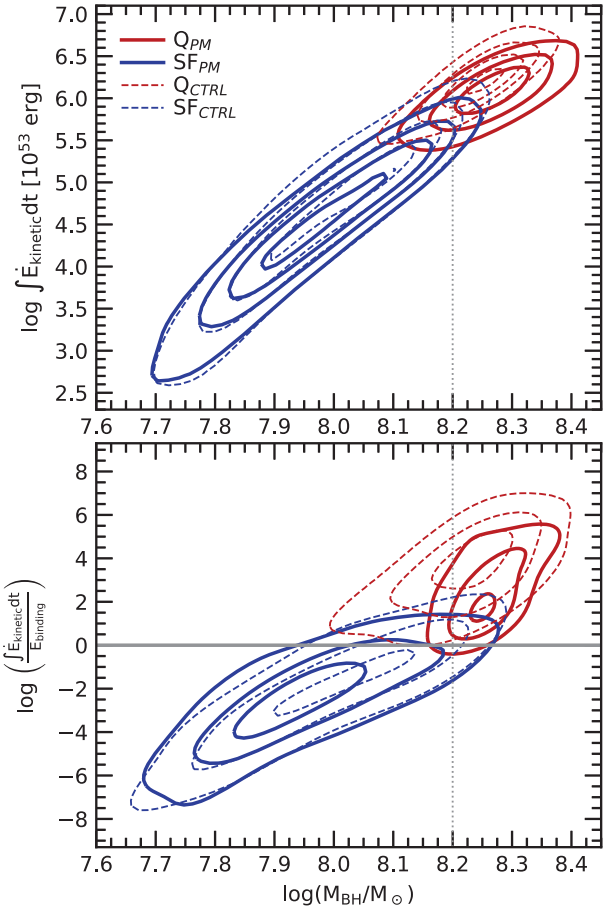

Figure 8. Top: the cumulative kinetic energy injected in the gas surrounding the central black hole as a function of black hole mass. Bottom: the ratio between the cumulative kinetic energy and the total gravitational binding energy of the gas, as a function of black hole mass. The post-merger galaxies are represented by solid contours: red for quenched post-mergers ($Q_{\rm PM}$ galaxies), and blue for star-forming post-mergers (SF$_{\rm PM}$ galaxies). Control galaxies are represented by dashed contours: red for quenched control galaxies ($Q_{\rm CTRL}$ galaxies), and blue for star-forming control galaxies (SF$_{\rm CTRL}$). The vertical dotted grey line at $M_{\rm BH} = 10^{8.2}$ M$_\odot$ represents the mass threshold above which more than 90 per cent of TNG galaxies are quenched (e.g. Zinger et al. 2020). The figure indicates that a necessary condition for star formation quenching in TNG galaxies is that the cumulative kinetic energy from the AGN feedback must overcome the total gravitational binding energy that keeps the gas bound to the galaxy.

Terrazas et al. (2020) show that the additional key ingredient necessary to understand star formation quenching in TNG galaxies is the proportion between the total amount of energy released into the gas via AGN kinetic feedback and the total gravitational energy felt by the gas cells. Indeed, Terrazas et al. (2020) showed that TNG galaxies whose kinetic energy overcomes the binding energy are typically quenched because the feedback has enough energy to push the gas out from the galaxies.

In the bottom panel of Fig. 8, we show the ratio between the total amount of energy released into the gas via AGN kinetic feedback and the total gravitational energy of the gas cells ($\frac{\int \dot{E}_{\rm kinetic}\,{\rm d}t}{E_{\rm binding}}$), as a function of black hole mass. We find that the TNG post-mergers and controls follow the same trend, with a sharp transition when the kinetic energy overtakes the binding energy of the gas. In ∼99 per cent of quenched post-mergers and in all quenched control galaxies the total

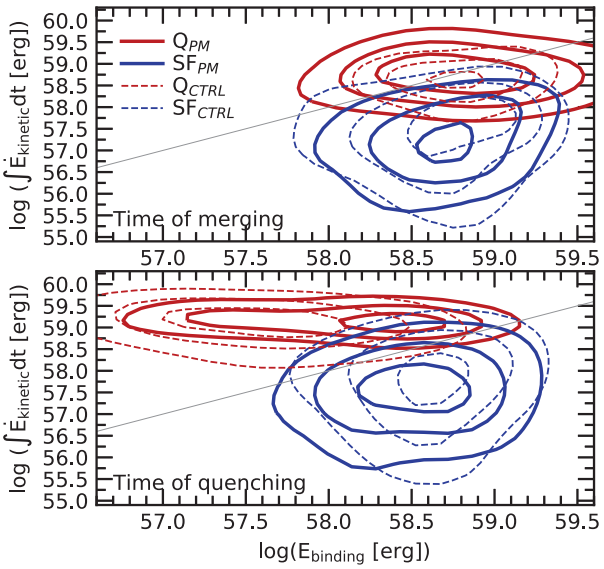

Figure 9. Top: the relation between the cumulative energy injected in the medium from the AGN activity as kinetic feedback (from the time when the black hole is seeded in the centre of the galaxy to $t_{\rm PM} = 0$) and the total binding energy of the gas particles at $t_{\rm PM} = 0$. Bottom: the same relation but at the time of quenching. The post-merger galaxies are represented by solid contours: red for quenched post-mergers ($Q_{\rm PM}$ galaxies), and blue for star-forming post-mergers ($\rm SF_{PM}$ galaxies). Control galaxies are represented by dashed contours: red for quenched control galaxies ($Q_{\rm CTRL}$ galaxies), and blue for star-forming control galaxies ($\rm SF_{CTRL}$). The grey line represents the bisector at which the cumulative binding energy equals the total binding energy. The figure shows that in $Q_{\rm PM}$ and $Q_{\rm CTRL}$ galaxies the binding energy decreases steadily, whilst the total kinetic feedback only slightly increases.

kinetic energy is higher than the binding energy, in contrast to only ∼12.7 per cent of star-forming post-mergers and ∼22.7 per cent of star-forming control galaxies. Therefore, the distinction between quenched and still star-forming galaxies is cleaner when binding energy is considered, as already reported by Terrazas et al. (2020). However, closer analysis of the bottom panel of Fig. 8 shows that there are some differences between quenched post-mergers and quenched control galaxies. At fixed $M_{\rm BH}$, quenched post-merger galaxies have, on average, lower $\frac{\int \dot{E}_{\rm kinetic}\,{\rm d}t}{E_{\rm binding}}$ than quenched control galaxies, thus suggesting they have higher binding energy (because quenched post-mergers and quenched control galaxies have similar cumulative kinetic energy, see the top panel of Fig. 8). Another difference between quenched post-merger and control populations is that there is a tail of quenched control galaxies with $M_{\rm BH} < 10^{8.2}\,{\rm M}_{\odot}$. We recall that the definition of quenched control galaxies includes all the quenched controls, hence the quenched control population represents the behaviour of the whole TNG quenched population. Therefore, though rare, there are quenched galaxies with black hole masses below the typical TNG mass threshold.

The results in Fig. 8 represent the instantaneous situation at the moment of quenching in the quenched post-merger population. It is instructive to observe how the two energy types evolve with time. Fig. 9 shows the relation between the cumulative kinetic energy and the binding energy at $t_{\rm PM} = 0$ (top panel) and at the time of the quenching (bottom panel): red for quenched post-mergers ($Q_{\rm PM}$ galaxies), and blue for star-forming post-mergers ($\rm SF_{PM}$ galaxies). Control galaxies are represented by dashed contours: red for quenched control galaxies ($Q_{\rm CTRL}$ galaxies), and blue for star-forming control galaxies ($\rm SF_{CTRL}$).

At $t_{\rm PM} = 0$ (Fig. 9, top panel), we find the quenched post-mergers and quenched control galaxies show, on average, similar values of binding and kinetic energies. Conversely, for the star-forming post-mergers and star-forming control galaxies the binding energy is larger than the kinetic energy, hence the gas is retained for ongoing star formation. Instead, at the time of quenching (Fig. 9, bottom panel), we find that both quenched post-mergers and quenched control galaxies have reduced binding energy, by typically −0.5 dex for quenched post-mergers and −1.1 dex for quenched control galaxies, while increasing their kinetic energy by ∼0.3 dex.

Following the evolution of the two energy types (as in Fig. 9) between $t_{\rm PM} = 0$ and the time of quenching, we find that the binding energy decreases steadily, while the total kinetic feedback only slightly increases. It is worth noting that there is a significant fraction of star-forming galaxies that exhibit an energetic ratio $\frac{\int \dot{E}_{\rm kinetic}\,{\rm d}t}{E_{\rm binding}} > 1$, as the quenched populations (see bottom panels of Figs 8 and 9). This means that the energy balance between kinetic and binding energies is not by itself a sufficient condition for quenching in TNG galaxies. By definition (see equation 1), the binding energy is proportional to the amount of gas in the reservoir of the galaxies. Consequently, it is expected that the binding energy decreases subject to the high gas loss we find in the quenched galaxy population in TNG (see Section 3.2). Moreover, the binding energy of the gas depends also on the strength of the gravitational potential, hence on the global mass distribution. Therefore, the binding energy, by definition, reflects the gas fraction in galaxies.

Fig. 10 shows the relation between the energetic ratio $\frac{\int \dot{E}_{\rm kinetic}\,{\rm d}t}{E_{\rm binding}}$ and the gas fraction (i.e. the fraction of the whole gas mass over the baryonic mass, $f_{\rm gas}$) at the time $t_{\rm PM} = 0$ of merging (top panel) and at the time of quenching (bottom panel). At the time of merging (Fig. 10, top panel), when all our galaxies are still star forming, the gas fractions of the populations that will eventually quench (i.e. $Q_{\rm PM}$ and $Q_{\rm CTRL}$) are lower than those that remain star forming (i.e. $\rm SF_{PM}$ and $\rm SF_{CTRL}$). Quantitatively, ∼50 per cent of $Q_{\rm PM}$ and $Q_{\rm CTRL}$ galaxies have $f_{\rm gas} \lesssim 0.2$, whilst $\rm SF_{PM}$ and $\rm SF_{CTRL}$ galaxies have instead gas fraction in the range $0.2 \lesssim f_{\rm gas} \lesssim 0.5$. This fact suggests that there is a pre-disposition towards quenching if the gas fraction is low to start with.

At the time of quenching (Fig. 10, bottom panel), the separation between the quenched and star-forming populations is seen as a very sharp distinction in gas fraction. We find a gas fraction threshold at roughly $f_{\rm gas} < 0.1$, below which all the TNG galaxies are quenched, and above which more than 98 per cent of galaxies are still star forming. Therefore, the gas fraction is a better discriminator than the energy ratio between TNG quenched and star-forming galaxies.

In summary of this section, we find that quenching is rare amongst post-mergers, although still more frequent than in the control sample. The quenching process in both the post-mergers and controls is linked to loss of gas that is triggered by AGN feedback. The star formation quenching dominates when the gas fraction is below $f_{\rm gas} \lesssim 0.1$.

4 IMPACT OF $M_{\rm BH}$ MATCHING SCHEME

A key part of our experimental set-up is the construction of the control sample. Our fiducial scheme includes matching in stellar mass, SFR, environment, and black hole mass. In particular, in order to limit any bias related to AGN in post-mergers and their controls, our matching criteria include a maximum tolerance of 0.05 dex (i.e. ∼12 per cent) on black hole mass of control galaxies (see Section 2). None the less, we find an excess of quenched galaxies in post-mergers compared to control galaxies that have not experienced any merger

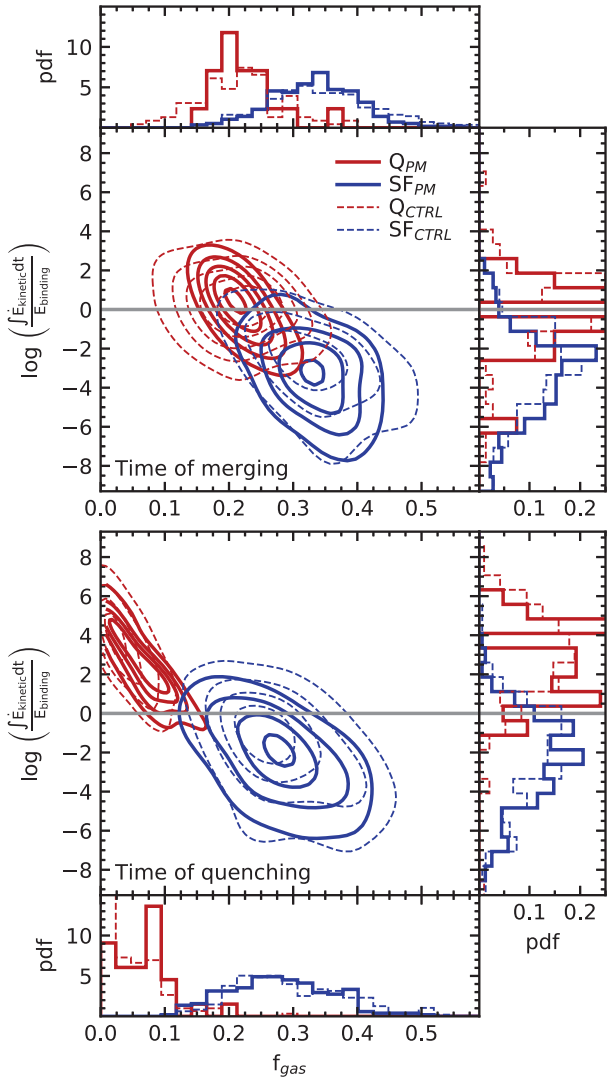

Figure 10. Top: the ratio between the cumulative kinetic energy (released from the time when the black hole is seeded in the centre of the galaxy to the time of coalescence $t_{PM} = 0$) and the total gravitational binding energy of the gas at $t_{PM} = 0$, as a function of the gas fraction at $t_{PM} = 0$. Bottom: the same relation but at the time of quenching (in the cases of the Q_{PM} and Q_{CTRL} populations), or $t_{PM} = 500$ Myr (in the cases of the SF_{PM} and SF_{CTRL} populations). The post-merger galaxies are represented by solid contours: red for quenched post-mergers (Q_{PM} galaxies), and blue for star-forming post-mergers (SF_{PM} galaxies). Control galaxies are represented by dashed contours: red for quenched control galaxies (Q_{CTRL} galaxies), and blue for star-forming control galaxies (SF_{CTRL}). The figure demonstrates that TNG post-merger galaxies (but also non-post-merger galaxies) quench when their gas fraction is below roughly 0.1.

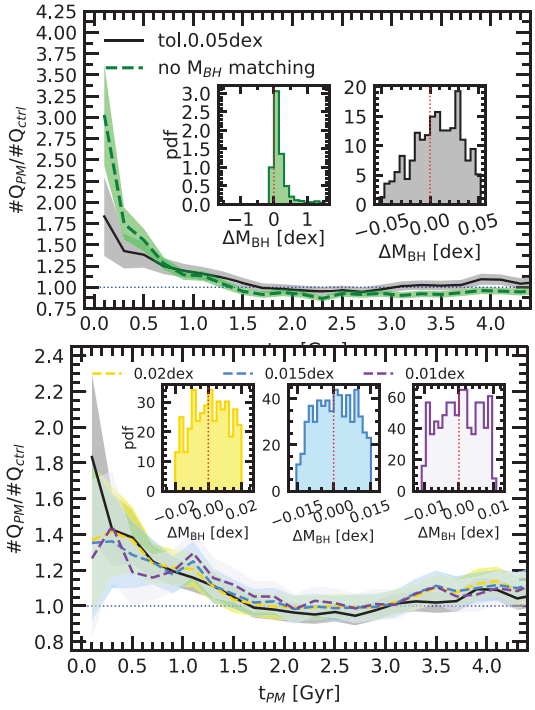

Figure 11. The ratios between the number of quenched post-mergers (Q_{PM}) and quenched controls (Q_{CTRL}) as a function of time elapsed since coalescence t_{PM}. The black curve and grey contours in both panels represent the reference result we show in Fig. 4, corresponding to a maximum tolerance of 0.05 dex (i.e. ∼12 per cent) in the match of black hole masses of control galaxies. The green curve in the top panel represents the ratio when none black hole matching criterion is applied. The coloured curves in the bottom represent the ratio relative to three tighter tolerance limits than that we choose in our analysis: yellow for a maximum mismatch of 0.02 dex (i.e. within 5 per cent), blue for 0.015 dex (i.e. a maximum mismatch of 3.5 per cent), and purple for 0.01 dex (i.e. within 2.3 per cent). The insets in each panel show the distributions of ΔM_{BH} (i.e. M_{BH} of post-mergers – M_{BH} of controls). The figure demonstrates that TNG post-mergers have a higher chance to quench the star formation in the early stages after coalescence compared to non-post-merger galaxies with similar characteristics and environment. The excess of quenched post-mergers cannot be simply ascribed to a mismatch in the black hole mass of the two populations.

in the last 2 Gyr. Therefore, it is worth investigating whether the excess is real or if it depends on the chosen M_{BH} tolerance, or in other words, to what extent the M_{BH} matching could bias our results.

In order to test the impact of our matching scheme, we remeasure the excess of post-mergers for different M_{BH} matching tolerances. We first remove any restrictions on M_{BH} in our search for control galaxies, then we selected three further control samples with more stringent tolerance in the M_{BH} difference than in the fiducial case, with 0.02 dex (i.e. a maximum mismatch around 5 per cent), 0.015 dex (i.e. a maximum mismatch of roughly 3.5 per cent), and 0.01 dex (i.e. a maximum mismatch of about 2.3 per cent).The top panel of Fig. 11 shows the ratio between the number of quenched post-mergers and quenched control galaxies matched without any restrictions on M_{BH}, while the bottom panel of Fig. 11 shows the same ratio for each of the three cases with more stringent tolerance on M_{BH} match. As a reference, in both panels we also display the ratio obtained with our fiducial tolerance, as in Fig. 4. We find that the different matchings show qualitatively consistent results, with an excess of quenched post-mergers immediately after coalescence followed by a steadily decreasing ratio with the time passed after the merger. Therefore, our qualitative conclusion that mergers lead to an excess of quenched galaxies are robust against the choice of the tolerance criterion on M_{BH}. However, changing the matching tolerance has a quantitative effect on the quenched fraction in the two populations. In the case where we do not match in black hole mass, we find a larger excess immediately after the coalescence phase (i.e. ≤160 Myr after the merger) compared to Section 3.1. The excess of quenched galaxies when no M_{BH} matching is used is

3 ± 0.6 times, at a significance level of 3.3σ (where σ represents the Poissonian error of the ratio). In the three cases with lower tolerances, the excess is 1.4 ± 0.6 times the number of $Q_{\rm CTRL}$ galaxies in all the three cases, only slightly smaller than the excess referred to the fiducial case, and the excess is confirmed at a significance level of $\sim 1\sigma$. We point out that by requiring more stringent constraints on the black hole mass of the control galaxies, we reduce the chance of finding a control galaxy for each post-merger, with the drawback of worsening the statistics of our result. Indeed, only 3 per cent of TNG post-mergers have a control galaxy that can be matched in $M_{\rm BH}$ with a tolerance of 0.01 dex. However, we find consistent trends for all tolerances considered, thus suggesting that the excess in the early phase after the merger would be present even with more extreme constraints on $M_{\rm BH}$ of matched control galaxies.

We next investigate the origin of the larger excess of post-mergers in the case without matching on black hole mass. Since AGN feedback is the driver of quenching in TNG, we expect that the higher fraction of quenched post-mergers compared with control galaxies should be related to an excess of post-mergers with $M_{\rm BH} \geq 10^{8.2}$ M$_\odot$, that is the black hole mass threshold above which more than 90 per cent of the TNG galaxies are quenched (see Section 3.3) and that can sustain efficient kinetic feedback. The inset panels in Fig. 11 show the distributions of the difference between the $M_{\rm BH}$ of TNG post-mergers that have $M_{\rm BH} \geq 10^{8.2}$ M$_\odot$ and their controls ($\Delta M_{\rm BH} = M_{\rm BH}$ of post-mergers – $M_{\rm BH}$ of controls). When we do not match in black hole mass, we find a skewed $\Delta M_{\rm BH}$ distribution, with almost all the post-mergers with $M_{\rm BH} \geq 10^{8.2}$ M$_\odot$ matched to control galaxies with lower black hole mass. The median of the distribution is $\Delta M_{\rm BH} = 0.11$ dex, but the high-end tail of the distribution show that $\sim$5 per cent of post-mergers with massive black holes have $\Delta M_{\rm BH} > 1$ dex, thus matched to controls whose black hole activity cannot sustain efficient AGN kinetic feedback. This test suggests that post-mergers with high-mass black holes have less chance to be matched to a control with comparable black hole mass. In other words, post-mergers could have a tendency to have higher black hole mass at fixed stellar mass than the non-post-merger population, which is what we might expect if mergers lead to enhanced black hole accretion (Byrne-Mamahit et al., in preparation). The inset panels in Fig. 11 also show the $\Delta M_{\rm BH}$ distribution related to the fiducial case we use in the rest of this paper (i.e. $M_{\rm BH}$ tolerance of 0.05 dex, or $\sim$12 per cent) and the $\Delta M_{\rm BH}$ distributions of the three cases with progressively reduced tolerance on $M_{\rm BH}$ of control galaxies. The $\Delta M_{\rm BH}$ distribution of the reference case has a median at $\sim$0.01 dex. Therefore, also in the reference case there are slightly more post-mergers matched to controls with less massive black holes, however, with a maximum difference of only 0.05 dex in $M_{\rm BH}$, the AGN model guarantees control galaxies with similar AGN feedback. The $\Delta M_{\rm BH}$ distributions of the three cases with progressively reduced tolerance on $M_{\rm BH}$ of control galaxies are symmetric, further limiting any mismatch in $M_{\rm BH}$.

To summarize, the results presented in this section suggest that TNG post-mergers have a higher chance to quench the star formation in the early stages after coalescence compared to non-post-merger galaxies with similar characteristics and environment. The excess of quenched post-mergers cannot be simply ascribed to a mismatch in the black hole mass of the two populations. Indeed, the excess persists when we remove any matching on the black hole mass. Therefore, even if the quenching in TNG post-mergers is strictly connected to AGN activity (see Section 3.3), the dynamics of galactic mergers could contribute to halting star formation in post-mergers.

5 RESOLUTION EFFECTS

In the work presented thus far, we exclusively analyse the evolution of post-mergers from TNG300-1. TNG300-1 offers the most robust statistics (a larger number of post-mergers) while maintaining a reasonable spatial and mass resolution. In this section, we perform a convergence test to investigate the robustness of our results against changes in the simulation's resolution (see Pillepich et al. 2018a for details about the convergence of the IllustrisTNG physical model). IllustrisTNG offers two other flagship simulations that use the same physical model but have different spatial and mass resolutions. The simulation TNG100-1 has 2×2500^3 resolution elements, and a dark matter particle mass resolution of $m_{\rm dm} = 7.5 \times 10^6$ M$_\odot$ and a baryonic target mass $m_{\rm bar} = 6 \times 10^6$ M$_\odot$, respectively, which corresponds to approximately an order of magnitude better spatial and mass resolution than TNG300-1. TNG100-1 simulates a smaller volume of 110.7^3 Mpc^3 that is around 1/20th of the volume simulated in TNG300-1 (see Section 2.1). The second simulation, TNG100-2, has the same volume as TNG100-1, but roughly the same mass and spatial resolutions as TNG300-1. Analysing the three simulations allows us to perform a test on the robustness of our results against distinct spatial and mass resolutions.

We note that TNG100-1 includes a total of 1855 post-mergers in the redshift range between $0 \leq z \leq 1$, whereas TNG300-1 provides a sample of 25 836 post-mergers (see Hani et al. 2020). By applying to TNG100-1 the same matching prescription we use for TNG300-1 (that consists of finding a control sample to the star-forming post-mergers with a match in the six parameters of redshift, stellar mass, SFR, N_2, r_1, and $M_{\rm BH}$), we would find control galaxies for only 64 star-forming post-mergers (compared with 3472 in TNG300-1). We find that the requirement on $M_{\rm BH}$ is the one that most significantly reduces the yields of controls. However, in Section 4 we showed that including a match in black hole mass only impacts the excess of quenched post-mergers slightly, therefore, to increase the number of star-forming post-mergers in TNG100-1 and TNG100-2 and improve the statistics of the result, we compare the behaviour of the three simulations without matching the control samples in black hole mass, but only in the other five aforementioned parameters. This way, we obtain a sample of 252 and 261 star-forming post-mergers in TNG100-1 and TNG100-2, respectively.

Fig. 12 shows the ratio between the number of quenched post-mergers ($Q_{\rm PM}$) and quenched control galaxies ($Q_{\rm CTRL}$) as a function of $t_{\rm PM}$ for the three TNG simulations. TNG300-1 and TNG100-2, the two simulations at a similar numerical resolution, show a very similar result, thus the reduced volume in TNG100-2 has little impact on the results other than poorer statistics (i.e. larger errors in the $Q_{\rm PM}/Q_{\rm CTRL}$ ratio). TNG100-1 shows qualitatively similar results to the lower resolution counterparts, with a grater excess (at a 1σ significance level) of quenched post-merger galaxies with respect to the quenched control sample. The difference in $Q_{\rm PM}/Q_{\rm CTRL}$ between the two resolution levels arises from a larger percentage of post-mergers that quench in the early phase after coalescence in the higher resolution simulation (TNG100-1). Around 250 Myr after coalescence we find that $\sim$7 per cent of post-mergers are quenched in TNG100-1, compared to $\sim$3 per cent in TNG300-1 and $\sim$4 per cent in TNG100-2, while the quenched fraction in the control samples is comparable regardless of the simulation's resolution ($\sim$1.5 per cent). Understanding the dependence of $Q_{\rm PM}/Q_{\rm CTRL}$ on the simulation's resolution is beyond the scope of this work. None the less, qualitatively all the three simulations offer compatible results, suggesting that our findings are robust to changes in the simulations' mass and spatial resolutions.

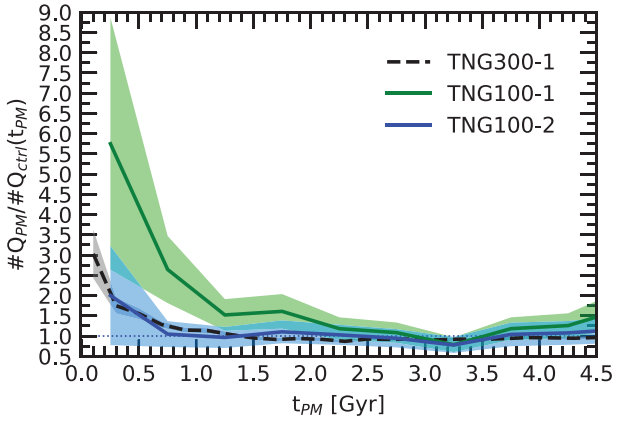

Figure 12. The ratio between the number of quenched post-mergers ($Q_{\rm PM}$) and quenched controls ($Q_{\rm CTRL}$) as a function of time elapsed since coalescence ($t_{\rm PM}$) for three TNG simulations at different mass and spatial resolutions, and different volumes. The black curve and grey shading represent the result from TNG300-1 without any match in black hole mass. The green solid curve with light green shading and the blue solid curve with light blue shading represent the ratios obtained from TNG100-1 and TNG100-2, respectively. To improve the statistics, the ratios from TNG100-1 and TNG100-2 are evaluated in bins of $t_{\rm PM}$ 500 Myr instead of $t_{\rm PM}$ 160 Myr as is done for TNG300-1. The figure reveals that the resolution of the simulation significantly affects the result, whilst the volume of the distribution affects only the statistics of the result but not the trend.

6 SUMMARY AND CONCLUSIONS

In this work, we present an analysis of the incidence and the causes of quenching in IllustrisTNG post-merger galaxies. We quantify the impact of single mergers on quenching star formation within 500 Myr after coalescence. We follow the evolution of the SFR in the post-merger descendants, and we compare the evolution to that of a control sample of non-post-merger galaxies matched in redshift, stellar mass, SFR, black hole mass, environment, and isolation. Our findings can be summarized as follows.

(i) *Quenching in TNG post-mergers*. Quenching is rare among the descendants of star-forming post-merger galaxies. Only around 5 per cent of TNG post-merger galaxies quench within 500 Myr after merging (see Fig. 3).

(ii) *The excess of quenched post-mergers*. Although quenching in post-mergers is rare, quenching occurs in post-mergers at twice the rate of the controls (see Fig. 4), i.e. 2.4 per cent of the control sample is quenched within 500 Myr.
The excess of quenched galaxies within the post-merger sample dissipates with time post-merger. After ∼1.5 Gyr, the post-merger quenched population is statistically indistinguishable from the control's quenched population (see Section 3.1).

(iii) *The effect of AGN feedback*. The kinetic mode of AGN feedback is responsible for quenching post-mergers in the TNG model. The feedback acts in two ways: (1) the kinetic feedback injects momentum into the gas particles surrounding the central black hole, thus ejecting the gas from the galaxy (ejective feedback, see Fig. 6), and (2) the kinetic feedback also prevents the gas from cooling to replenish the galactic reservoir for sustaining new episodes of star formation (preventive feedback, see Section 3.2). Quenching is most effective in galaxies with $M_{\rm BH} \gtrsim 10^{8.2}$ M$_\odot$. At black hole masses higher than $M_{\rm BH} \gtrsim 10^{8.2}$ M$_\odot$ the total kinetic energy injected into the gas by the central black hole dominates over the gas's gravitational binding energy; as a result a notable fraction of the gas reservoir is removed from the galaxy (see Figs 8 and 9).

(iv) *Quenching and gas fraction*. We find that (1) there is a predisposition towards quenching if the gas fraction in a galaxy is low, and (2) the separation between the quenched and star-forming populations at the time of quenching is demarcated by a very sharp distinction in gas fraction, as quenched galaxies dominate at gas fractions below $f_{\rm gas} \sim 0.1$ (see Fig. 10).

(v) *The effect of different $M_{\rm BH}$ matching schemes*. The excess of quenched post-mergers with respect to the number of quenched galaxies in the control population is stronger when we do not include a matching criterion for the black hole mass. None the less, though slightly weaker, the excess persists also when we match control galaxies with a maximum tolerance of 0.015 dex in black hole mass (see Fig. 11).

The picture that arises from our analysis is that mergers in TNG do not contribute significantly to the quenching of star-forming galaxies. The rarity of quenching in post-mergers is qualitatively in accordance with other cosmological simulations and observational results. For instance, Rodríguez Montero et al. (2019) find that major mergers in the SIMBA simulation (Davé et al. 2019) are not directly related to quenching, as the typical delay between the merger and subsequent quenching is larger than 1 Gyr. By analysing a sample of galaxies extracted from the Sloan Digital Sky Survey (SDSS) Data Release 7 (DR7), Weigel et al. (2017) show that major mergers should not be the preferred path leading to permanent quenching. They found that major merger quenched galaxies account for a maximum of 5 per cent of the quenched population at a given stellar mass, both at low and intermediate redshift.

Despite the small absolute fraction of promptly quenched galaxies, there is a notable excess of quenched post-mergers compared to the control population, thus suggesting that mergers could have a non-negligible contribution to the quenching of star formation. Mergers disturb the internal kinematics of the galaxy (i.e. dark matter, stars, gas). The induced turbulence in the ISM could dissipate angular momentum of the infalling gas, and we are investigating this process in TNG post-mergers in a follow-up project. Gas infalling with reduced angular momentum could reach the centres of the galaxies and feed the central black holes. The temporary excess of quenched post-mergers found in the early phase after coalescence completely vanishes after ∼1.5 Gyr following the merger, suggesting that the mergers accelerate the quenching process in those post-mergers whose progenitors were close to sustaining effective AGN kinetic feedback.

Our results may be dependent on the AGN feedback model implemented in IllustrisTNG. However, the dynamics of galactic mergers could contribute to halting star formation in post-mergers for a variety of reasons. For example, Pontzen et al. (2017) applied a genetic modification approach (Roth, Pontzen & Peiris 2016) to generate sets of controlled numerical realizations in a fully cosmological context of a halo of 10^{12} M$_\odot$, by altering its accretion history. They find that in major mergers (a mass ratio of 2:3) AGN feedback alone is not sufficient to permanently quench star formation, but it acts in synergy with the kinetic effects of the merger. The interaction disrupts the gaseous disc of the galaxy, resulting in a turbulent medium able to remove angular momentum from inflowing material; then, the inflowing material can easily reach the galactic centre to feed the black hole and the subsequent AGN activity contributes significantly to removing the remaining gas from the galaxy (see also Chadayammuri et al. 2020). More recently, Sanchez et al. (2020) used a similar approach to analyse the impact

of minor mergers on the star formation of simulated Milky Way analogues. They find that two small satellites interacting with the host can quench a Milky Way-like galaxy. The mechanism is similar to the one in Pontzen et al. (2017), but in this case, it requires a tandem operation of a merger with the first satellite and subsequent close interaction with the second satellite to disrupt the gaseous disc and trigger intense AGN activity to halt the star formation. In a follow-up project, we will statistically analyse the repercussions of multiple interactions/mergers on quenching in large cosmological simulations. In a follow-up project, in order to gain new insights on the impact of mergers on quenching, we will analyse other cosmological simulations that implement different models to regulate black hole accretion, such as the EAGLE simulation (Schaye et al. 2015) and the Illustris simulation (Vogelsberger et al. 2014).

ACKNOWLEDGEMENTS

The authors are grateful to Dan Walters and Brian A. Terrazas for useful discussions. SQ is also grateful to Lucia Pozzetti, Douglas Rennehan, and Isabel Santos Santos for helpful discussion and suggestions. MHH acknowledges support from the William and Caroline Herschel Postdoctoral Fellowship fund, and the Vanier Canada Graduate Scholarship. DRP and SLE gratefully acknowledge NSERC for Discovery Grants that helped to fund this research. The simulations of the IllustrisTNG project used in this work were undertaken with compute time awarded by the Gauss Centre for Supercomputing (GCS) under GCS Large-Scale Projects GCS-ILLU and GCS-DWAR on the GCS share of the supercomputer Hazel Hen at the High Performance Computing Center Stuttgart (HLRS), as well as on the machines of the Max Planck Computing and Data Facility (MPCDF) in Garching, Germany. This research was enabled, in part, by the computing resources provided by WestGrid and Compute Canada.

DATA AVAILABILITY

The data used in this work are publicly available at https://www.tng-project.org.

REFERENCES

Baldry I. K., Glazebrook K., Brinkmann J., Ivezić Ž., Lupton R. H., Nichol R. C., Szalay A. S., 2004, ApJ, 600, 681
Balogh M. L., Baldry I. K., Nichol R., Miller C., Bower R., Glazebrook K., 2004, ApJ, 615, L101
Bekki K., 2009, MNRAS, 399, 2221
Bell E. F. et al., 2004, ApJ, 600, L11
Bell E. F. et al., 2012, ApJ, 753, 167
Benson A. J., 2012, New Astron., 17, 175
Blanton M. R. et al., 2003, ApJ, 594, 186
Bower R. G., Benson A. J., Malbon R., Helly J. C., Frenk C. S., Baugh C. M., Cole S., Lacey C. G., 2006, MNRAS, 370, 645
Boylan-Kolchin M., Springel V., White S. D. M., Jenkins A., Lemson G., 2009, MNRAS, 398, 1150
Bradford J. D., Geha M. C., Greene J. E., Reines A. E., Dickey C. M., 2018, ApJ, 861, 50
Cattaneo A. et al., 2009, Nature, 460, 213
Chabrier G., 2003, PASP, 115, 763
Chadayammuri U., Tremmel M., Nagai D., Babul A., Quinn T., 2021, MNRAS, preprint (arXiv:2001.06532)
Cheung E. et al., 2012, ApJ, 760, 131
Cimatti A. et al., 2013, ApJ, 779, L13
Conselice C. J., 2014, ARA&A, 52, 291
Crenshaw D. M., Schmitt H. R., Kraemer S. B., Mushotzky R. F., Dunn J. P., 2010, ApJ, 708, 419
Croton D. J. et al., 2006, MNRAS, 365, 11
Davé R., Anglés-Alcázar D., Narayanan D., Li Q., Rafieferantsoa M. H., Appleby S., 2019, MNRAS, 486, 2827
Dekel A., Birnboim Y., 2008, MNRAS, 383, 119
de Ravel L. et al., 2009, A&A, 498, 379
Di Matteo T., Springel V., Hernquist L., 2005, Nature, 433, 604
Di Matteo P., Combes F., Melchior A.-L., Semelin B., 2007, A&A, 468, 61
Drory N., Bender R., Feulner G., Hopp U., Maraston C., Snigula J., Hill G. J., 2004, ApJ, 608, 742
Ellison S. L., Patton D. R., Simard L., McConnachie A. W., 2008, AJ, 135, 1877
Ellison S. L., Mendel J. T., Patton D. R., Scudder J. M., 2013, MNRAS, 435, 3627
Ellison S. L., Viswanathan A., Patton D. R., Bottrell C., McConnachie A. W., Gwyn S., Cuillandre J.-C., 2019, MNRAS, 487, 2491
Faber S. M. et al., 2007, ApJ, 665, 265
Fabian A. C., 2012, ARA&A, 50, 455
Gensior J., Kruijssen J. M. D., 2021, MNRAS, 500, 2000
Gensior J., Kruijssen J. M. D., Keller B. W., 2020, MNRAS, 495, 199
Goto T., Yamauchi C., Fujita Y., Okamura S., Sekiguchi M., Smail I., Bernardi M., Gomez P. L., 2003, MNRAS, 346, 601
Gunn J. E., Gott J. R., III, 1972, ApJ, 176, 1
Hani M. H., Gosain H., Ellison S. L., Patton D. R., Torrey P., 2020, MNRAS, 493, 3716
Hopkins P. F., Hernquist L., Cox T. J., Kereš D., 2008, ApJS, 175, 356
Ilbert O. et al., 2010, ApJ, 709, 644
Ilbert O. et al., 2013, A&A, 556, A55
Jarvis M. E. et al., 2020, MNRAS, 498, 1560
Jogee S. et al., 2009, ApJ, 697, 1971
Kauffmann G. et al., 2003, MNRAS, 341, 54
Kaviraj S., Kirkby L. A., Silk J., Sarzi M., 2007, MNRAS, 382, 960
Kennicutt Robert C. J., 1998, ApJ, 498, 541
Khalatyan A., Cattaneo A., Schramm M., Gottlöber S., Steinmetz M., Wisotzki L., 2008, MNRAS, 387, 13
Knapen J. H., Cisternas M., Querejeta M., 2015, MNRAS, 454, 1742
Koss M. J. et al., 2021, ApJS, 252, 29
Larson R. B., Tinsley B. M., Caldwell C. N., 1980, ApJ, 237, 692
Li C., Kauffmann G., Heckman T. M., Jing Y. P., White S. D. M., 2008, MNRAS, 385, 1903
Lin L. et al., 2007, ApJ, 660, L51
Lin L. et al., 2008, ApJ, 681, 232
López-Sanjuan C. et al., 2013, A&A, 553, A78
Lotz J. M., Jonsson P., Cox T. J., Croton D., Primack J. R., Somerville R. S., Stewart K., 2011, ApJ, 742, 103
Lu Y., Mo H. J., Weinberg M. D., Katz N., 2011, MNRAS, 416, 1949
McNamara B. R., Nulsen P. E. J., 2007, ARA&A, 45, 117
Marinacci F. et al., 2018, MNRAS, 480, 5113
Martig M., Bournaud F., Teyssier R., Dekel A., 2009, ApJ, 707, 250
Mihos J. C., Hernquist L., 1996, ApJ, 464, 641
Moore B., Lake G., Katz N., 1998, ApJ, 495, 139
Muzzin A. et al., 2013, ApJS, 206, 8
Naiman J. P. et al., 2018, MNRAS, 477, 1206
Nelson D. et al., 2015, Astron. Comput., 13, 12
Nelson D. et al., 2018, MNRAS, 475, 624
Nelson D. et al., 2019, Comput. Astrophys. Cosmol., 6, 2
Pakmor R., Springel V., Bauer A., Mocz P., Munoz D. J., Ohlmann S. T., Schaal K., Zhu C., 2016, MNRAS, 455, 1134
Patton D. R., Grant J. K., Simard L., Pritchet C. J., Carlberg R. G., Borne K. D., 2005, AJ, 130, 2043
Patton D. R., Torrey P., Ellison S. L., Mendel J. T., Scudder J. M., 2013, MNRAS, 433, L59
Patton D. R., Qamar F. D., Ellison S. L., Bluck A. F. L., Simard L., Mendel J. T., Moreno J., Torrey P., 2016, MNRAS, 461, 2589
Patton D. R. et al., 2020, MNRAS, 494, 4969
Peng Y.-j., Lilly S. J., Renzini A., Carollo M., 2012, ApJ, 757, 4
Peng Y.-j. et al., 2010, ApJ, 721, 193

Pillepich A. et al., 2018a, MNRAS, 473, 4077
Pillepich A. et al., 2018b, MNRAS, 475, 648
Planck Collaboration XIII, 2016, A&A, 594, A13
Pontzen A., Tremmel M., Roth N., Peiris H. V., Saintonge A., Volonteri M., Quinn T., Governato F., 2017, MNRAS, 465, 547
Pozzetti L. et al., 2010, A&A, 523, A13
Rodighiero G. et al., 2011, ApJ, 739, L40
Rodighiero G. et al., 2015, ApJ, 800, L10
Rodriguez-Gomez V. et al., 2015, MNRAS, 449, 49
Rodríguez Montero F., Davé R., Wild V., Anglés-Alcázar D., Narayanan D., 2019, MNRAS, 490, 2139
Roth N., Pontzen A., Peiris H. V., 2016, MNRAS, 455, 974
Sanchez N. N., Tremmel M., Werk J. K., Pontzen A., Christensen C., Quinn T., Loebman S., Cruz A., 2020, preprint (arXiv:2009.05581)
Schaye J. et al., 2015, MNRAS, 446, 521
Scudder J. M., Ellison S. L., Torrey P., Patton D. R., Mendel J. T., 2012, MNRAS, 426, 549
Shangguan J., Ho L. C., Xie Y., 2018, ApJ, 854, 158
Shangguan J., Ho L. C., Bauer F. E., Wang R., Treister E., 2020, ApJ, 899, 112
Sijacki D., Springel V., Di Matteo T., Hernquist L., 2007, MNRAS, 380, 877
Somerville R. S., Davé R., 2015, ARA&A, 53, 51
Somerville R. S., Hopkins P. F., Cox T. J., Robertson B. E., Hernquist L., 2008, MNRAS, 391, 481
Springel V., 2010, MNRAS, 401, 791
Springel V., Hernquist L., 2003, MNRAS, 339, 289
Springel V., Di Matteo T., Hernquist L., 2005a, MNRAS, 361, 776
Springel V. et al., 2005b, Nature, 435, 629
Springel V., Di Matteo T., Hernquist L., 2005c, ApJ, 620, L79
Springel V. et al., 2017, MNRAS, 475, 676
Strateva I. et al., 2001, AJ, 122, 1861
Tacchella S. et al., 2015, Science, 348, 314
Terrazas B. A. et al., 2020, MNRAS, 493, 1888
Thorp M. D., Ellison S. L., Simard L., Sánchez S. F., Antonio B., 2019, MNRAS, 482, L55
Villar-Martín M., Humphrey A., Delgado R. G., Colina L., Arribas S., 2011, MNRAS, 418, 2032
Vogelsberger M., Genel S., Sijacki D., Torrey P., Springel V., Hernquist L., 2013, MNRAS, 436, 3031
Vogelsberger M. et al., 2014, MNRAS, 444, 1518
Weigel A. K. et al., 2017, ApJ, 845, 145
Weinberger R. et al., 2017, MNRAS, 465, 3291
Weinberger R. et al., 2018, MNRAS, 479, 4056
Whitaker K. E. et al., 2011, ApJ, 735, 86
White S. D. M., Frenk C. S., 1991, ApJ, 379, 52
Willmer C. N. A. et al., 2006, ApJ, 647, 853
Wilson T. J. et al., 2019, ApJ, 874, 18
Wong K. C. et al., 2011, ApJ, 728, 119
Woo J., Dekel A., Faber S. M., Koo D. C., 2015, MNRAS, 448, 237
Woo J.-H., Bae H.-J., Son D., Karouzos M., 2016, ApJ, 817, 108
Woo J., Carollo C. M., Faber S. M., Dekel A., Tacchella S., 2017, MNRAS, 464, 1077
Wuyts S. et al., 2011, ApJ, 742, 96
Zinger E. et al., 2020, MNRAS, 499, 768

This paper has been typeset from a TEX/LATEX file prepared by the author.